Chapter 2

A Unified Analysis of Adhesive-Bonded Cylindrical Coupler Joints

Sontipee Aimmanee

Additional information is available at the end of the chapter

http://dx.doi.org/10.5772/intechopen.72288

Abstract

In the past years, many studies have been conducted on behaviors of adhesive tubular joints subjected to various loading conditions, such as torsion, axial, and internal and external pressure. However, the previous models are conceptually distinct, since they were developed to analyze only for each type of load. Mostly, homogeneous isotropic or orthotropic material were considered and thin-walled joint structures were examined. Therefore, the aim of this chapter is to present for the first time a generalized mathematical formulation and modeling of adhesive-bonded cylindrical coupler joints taking into account all loading scenarios. The inner and outer adherends can be made of isotropic, orthotropic, or laminated composite materials, and they are modeled as three-dimensional elastic body, so adherends with any thickness can be analyzed. Assumptions of an axisymmetric joint with linearly elastic adherends and adhesive materials are employed. Thin adhesive layer is considered so that only the out-of-plane adhesive stresses are concerned, and they are treated to be uniform through its thickness. Using elasticity theory and the newly developed finite-segmented method, stress distributions in both adherends and adhesive can be evaluated. Calculation examples of laminated composite joints are given. This model provides the unified analysis of adhesive-bonded cylindrical coupler joints.

Keywords: adhesive, coupler joint, lap joint, elasticity, finite-segment method

1. Introduction

Structures usually need to have joints connecting each part together due to the limitation of manufacturing, transportation, and installation. These structures are generally vulnerable at the joints because of the stress concentrations from material discontinuity. There are many types of joint, such as mechanical joints, welding joints, and adhesive-bonded joints. Over the other kinds of joints, adhesive-bonded joints have advantages due to less stress concentration,

higher capability of joining dissimilar materials, lighter weight, and better corrosion resistance. Nonetheless, stress concentration in the adhesive layer is still existing. The adhesive stress distribution is locally nonuniform and always highest at the edges of the bonding region. Thus, in order to use an adhesive-bonded joint safely, it is important to predict the developed adhesive stress accurately. A good analysis also provides the understanding of the joint behavior, yielding a design for improving the joint performance by decreasing the joint stress concentration.

There are lots of literature dealing with the stresses in lap joints and coupler joints between two tubular adherends. Among several types of adhesive-bonded joint, cylindrical or tubular joints subjected to axial, torsional, and external as well as internal pressure loads have been one of the main focus of mechanics of adhesion research for a half century due to their popular usage in many engineering applications. The analytical modeling and finite-element analysis are the two popular approaches for predicting the stresses developed in adhesive and adherends. In order to recognize the progress in this field, some examples of important work in mathematical modeling are given below.

For axial loads, the early investigation was conducted by Lubkin and Reissner [1] who analyzed the tubular lap joints. Axial shear stresses and radial normal stresses in the adhesive layer were predicted under the assumption of approximating the layer as an infinite number of tensile and shear springs. However, disappearance of axial shear stress on the free surfaces at the ends of the adhesive was not considered. Adam and Peppiatt [2] performed axisymmetric finite-element analysis (FEA) of tubular lap joints subjected to stretching and twisting loads. The effects of an adhesive filet and partial tapering adherends on stress distribution were also reported. Using a minimum strain energy, Allman [3] proposed two-dimensional analytical solution for lap joints that ensure the traction-free boundary condition. Bending, stretching, and shearing of the adherends and shearing and tearing of the adhesive layer were taken into account. Shi and Cheng [4] formulated closed-form solutions for tubular lap joints utilizing the variational principle of complementary energy. Boundary conditions and assumptions of Allman were adopted in their model development. Nemes et al. [5] further developed the stress analysis of adhesive in a cylindrical assembly of two tubes. Variational method of the potential energy was also employed. Nonetheless, Nemes et al. neglected radial stress component in the joint. Kumar [6] presented a theoretical framework for the stress analysis of shaft-tube adhesive joints subjected to tensile loads. The joint assembly was considered to consist of similar or dissimilar isotropic or orthotropic adherends. The principle of minimum complementary energy and a stress function approach were used to establish the governing equations in order to determine the stress state in each constituent. To reduce the stress concentration, Kumar [7] also studied the use of functionally graded adhesive in a tubular lap joint with an isotropic adherend under tension. In his model, the adhesive was divided into annular rings to take into account the gradient property of shear modulus.

Regarding the case of the tubular joint subjected to torsion, Volkersen [8] provided a closed-form solution for circumferential shear stresses at the interface of tubular lap joint exerted by a torque. Pugno and Surace [9] investigated the analysis of the joint subjected to torsion. They utilized the common function of resultant torques in adherends and achieved the uniform adhesive hoop shear stress by tapering adherend surfaces. Xu and Li [10] investigated the full

three-dimensional stress analysis of a bonded tubular-coupler joint subjected to torsion. Their purpose was to investigate all of the adherend and adhesive stress components without the assumption of through-thickness constant stresses across the adhesive layer. Oh [11] performed an analysis of the bonded tubular lap joint of laminated tubes with softening adhesive's stiffness properties under torsion using an elasticity model. Oh concluded that the load capacity in the linear analysis can be quite underestimated when compared to the nonlinear modeling. Spaggiari and Dragoni [12] investigated the joint studied in the Kumar's work in [7], but the joint is subjected to torsion instead. They developed the closed-form function of the adhesive shear modulus in order to minimize adhesive shear stress over the bonding region and addressed the limitation of shear modulus and thicknesses ratio for joint manufacturing with functionally graded adhesives. Recently, Aimmanee and Hongpimolmas [13] formulated a mathematical model of an adhesive-bonded tubular joint with a variable-stiffness composite coupler. The optimal variable fiber orientation in the coupler was determined to minimize the adhesive hoop shear stress.

Stresses in cylindrical joints under pressure have also been studied, even though investigation of this type of load was comparatively scarce compared to the above two loadings. Terekhova and Skoryi [14] provided a close-form solution for the stresses in tubular lap joints under external and internal pressures and axial forces. Their model neglected the effect of adherend bending. Baishya et al. [15] conducted research in individual and combined effect of internal pressure and torsional loading on stress and failure characteristics of tubular single lap joints made of composite materials. The onset of different joint fracture modes was investigated in their work. Strength analysis of adhesive joints of riser pipes in deep sea environment loadings was performed by Zhang et al. [16] External pressure, internal pressure, tension, torsion, and bending were examined to understand singular stress fields existing around end of the interface. Apalak [17] investigated elastic stresses in the adhesive layer and tubes of an adhesively bonded tubular joint with functionally graded tubes subjected to an internal pressure. Finite-element method was used to model the tubes having gradient layer between a ceramic layer and a metal layer.

According to the former analytical research work presented in the literature, the problems can be mathematically complicated even though the joint is made of simple conventional isotropic adherends. In addition, the previous models usually are distinct for each type of load, since they were developed to analyze only for a specific loading case. Therefore, this chapter aims to present a mathematical modeling of adhesive-bonded cylindrical coupler joints taking into account all loading scenarios, i.e., torsion, axial, and pressure loadings. The inner and outer adherends can be made of isotropic, orthotropic, or laminated composite materials, and they are modeled as three-dimensional elastic body, so a thick or solid cylinder adherend can also be analyzed. Stresses in adhesive layer and adherends can be evaluated by newly developed finite-segment method. The unified formulation of the model will be discussed in the next section.

2. Elasticity theory of a laminated cylindrical structure

A bonded-coupler joint is illustrated in **Figure 1(a)**. The joint consists of two inner tubes (adherend part 1), a coupler of length 2 L (or adherend part 2), and an adhesive layer. The

cylindrical coordinates (x, θ, r) depicted in **Figure 2** are used to describe the joint geometry. Because of symmetry about the cross-sectional plane in the middle, only half of the coupler joint is demonstrated in **Figure 1(b)**. Either half is equivalent to a single tubular lap joint and applicable for modeling and analysis. The inner tubes are considered to be made of an ordinary material, such as an isotropic metal or a more sophisticated material, namely, orthotropic material or laminated composite. On the contrary the coupler is proposed to be fabricated from a symmetric-balanced laminated composite with variable fiber orientation in the x direction.

For the sake of generality, this section discusses the elasticity theory of a laminated cylindrical tube [18]. A sketch of a general open-ended, cylindrical, laminated N-layer tube subjected to uniform loads is shown in **Figure 2**. Each layer is made of a unidirectional fiber-reinforced composite material. The principal material coordinates (1, 2, 3), whose axes are mutually orthogonal, are defined along the fiber orientation, tangent, and normal to the tube surface, respectively. The layers in the tube are perfectly bonded between each other. Evidently, this considered laminated cylinder can be simply degenerated into a single isotropic or orthotropic tube by letting $N = 1$ and employing the related elastic properties. For the tube with

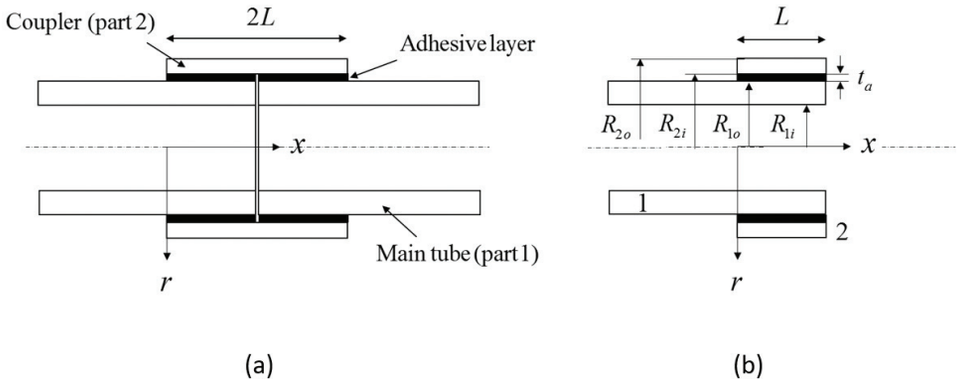

Figure 1. Schematic of a bonded-coupler joint: (a) full model and (b) half model or tubular lap joint model.

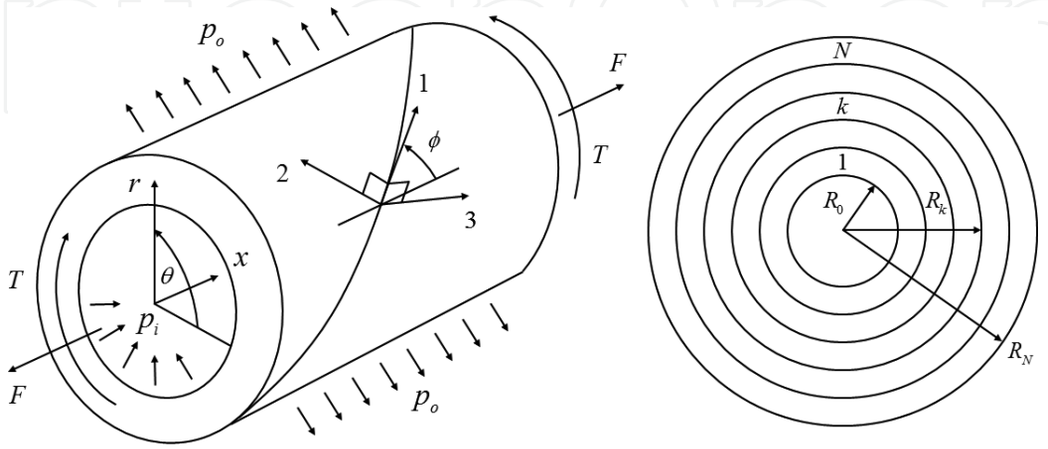

Figure 2. A laminated tube and the defined coordinate systems.

axisymmetric geometry and circumferentially independent material properties under a uniform load, the strain–displacement relations in the k^{th} layer in the cylindrical coordinates are

$$\begin{aligned} \varepsilon_x^{(k)} &= \frac{\partial u^{(k)}}{\partial x}, & \varepsilon_\theta^{(k)} &= \frac{w^{(k)}}{r}, & \varepsilon_r^{(k)} &= \frac{\partial w^{(k)}}{\partial r} \\ \gamma_{\theta r}^{(k)} &= \frac{\partial v^{(k)}}{\partial r} - \frac{v^{(k)}}{r}, & \gamma_{xr}^{(k)} &= \frac{\partial u^{(k)}}{\partial r}, & \gamma_{x\theta}^{(k)} &= \frac{\partial v^{(k)}}{\partial x} \end{aligned} \tag{1}$$

where ε and γ denote normal and shear strains, respectively. u, v, and w are displacements in axial, tangential, and radial directions, respectively. Superscript (k) indicates that the corresponding quantities are in the k^{th} layer.

According to the prescribed loading conditions and constant fiber orientation, the normal stresses, σ, and the shear stresses, τ, are independent of x and θ. The equilibrium equations in the k^{th} layer along the r-, θ-, x-directions are reduced to ordinary differential equations with respect to r, respectively, as

$$\frac{\partial \sigma_r^{(k)}}{\partial r} + \frac{1}{r}\left(\sigma_r^{(k)} - \sigma_\theta^{(k)}\right) = 0 \tag{2}$$

$$\frac{\partial \tau_{\theta r}^{(k)}}{\partial r} + \frac{2}{r}\tau_{\theta r}^{(k)} = 0 \tag{3}$$

$$\frac{\partial \tau_{xr}^{(k)}}{\partial r} + \frac{1}{r}\tau_{xr}^{(k)} = 0 \tag{4}$$

The stresses and strains in the k^{th} layer in (x, θ, r) coordinates expressed in Eqs. (1)–(4) can be transformed to those in the principal material coordinates (1, 2, 3) as follows:

$$\{\sigma\}_{123}^{(k)} = [T]^{(k)}\{\sigma\}_{x\theta r}^{(k)}, \qquad \{\varepsilon\}_{123}^{(k)} = [T]^{(k)}\{\varepsilon\}_{x\theta r}^{(k)} \tag{5}$$

where $\{\sigma\}_{123}^{(k)}$ and $\{\varepsilon\}_{123}^{(k)}$ are tensorial stress and tensorial strain components, respectively. $[T]^{(k)}$ is transformation matrix of the k^{th} layer as shown in Eq. (6), in which $m^{(k)} = \cos\varnothing^{(k)}$ and $n^{(k)} = \sin\varnothing^{(k)}$. $\varnothing^{(k)}$ is fiber angle of the k^{th} layer as shown in **Figure 2**.

$$[T]^{(k)} = \begin{bmatrix} \left(m^{(k)}\right)^2 & \left(n^{(k)}\right)^2 & 0 & 0 & 0 & 2m^{(k)}n^{(k)} \\ \left(n^{(k)}\right)^2 & \left(m^{(k)}\right)^2 & 0 & 0 & 0 & -2m^{(k)}n^{(k)} \\ 0 & 0 & 1 & 0 & 0 & 0 \\ 0 & 0 & 0 & m^{(k)} & -n^{(k)} & 0 \\ 0 & 0 & 0 & n^{(k)} & m^{(k)} & 0 \\ -m^{(k)}n^{(k)} & m^{(k)}n^{(k)} & 0 & 0 & 0 & \left(m^{(k)}\right)^2 - \left(n^{(k)}\right)^2 \end{bmatrix} \tag{6}$$

The constitutive relation in the k^{th} layer in the cylindrical coordinates can be written as

$$\{\sigma\}_{x\theta r}^{(k)} = \left[\overline{C}\right]^{(k)}\{\varepsilon^{eng}\}_{x\theta r}^{(k)} \tag{7}$$

In the above, $\left[\overline{C}\right]^{(k)}$ is the transformed stiffness matrix, and $\{\varepsilon^{eng}\}^{(k)}_{x\theta r}$ is engineering strain components in the global cylindrical coordinate system. The transformed stiffness matrix $\left[\overline{C}\right]^{(k)}$ can be evaluated as

$$\left[\overline{C}\right]^{(k)} = \left\{[T]^{(k)}\right\}^{-1}[C\,]^{(k)}[R\,][T]^{(k)}[R\,]^{-1} \tag{8}$$

where $[C\,]^{(k)}$, as shown in Eq. (9), is the stiffness matrix in the principle material coordinate system in the k^{th} layer.

$$[C\,]^{(k)} = \begin{bmatrix} 1/E_1^{(k)} & -\upsilon_{12}^{(k)}/E_1^{(k)} & -\upsilon_{31}^{(k)}/E_3^{(k)} & 0 & 0 & 0 \\ -\upsilon_{21}^{(k)}/E_2^{(k)} & 1/E_2^{(k)} & -\upsilon_{32}^{(k)}/E_3^{(k)} & 0 & 0 & 0 \\ -\upsilon_{13}^{(k)}/E_1^{(k)} & -\upsilon_{23}^{(k)}/E_2^{(k)} & 1/E_3^{(k)} & 0 & 0 & 0 \\ 0 & 0 & 0 & 1/G_{23}^{(k)} & 0 & 0 \\ 0 & 0 & 0 & 0 & 1/G_{13}^{(k)} & 0 \\ 0 & 0 & 0 & 0 & 0 & 1/G_{12}^{(k)} \end{bmatrix}^{-1} \tag{9}$$

$E^{(k)}$ and $G^{(k)}$ are Young's modulus and shear modulus, respectively. $[R\,]$ is the Reuter's matrix, which is defined as

$$[R\,] = \begin{bmatrix} 1 & 0 & 0 & 0 & 0 & 0 \\ 0 & 1 & 0 & 0 & 0 & 0 \\ 0 & 0 & 1 & 0 & 0 & 0 \\ 0 & 0 & 0 & 2 & 0 & 0 \\ 0 & 0 & 0 & 0 & 2 & 0 \\ 0 & 0 & 0 & 0 & 0 & 2 \end{bmatrix} \tag{10}$$

With the strains defined in Eq. (1), three out of six equations of the compatibility in the cylindrical coordinates described in [19] are automatically satisfied. Solving the equilibrium equations in Eqs. (2)–(4) and using the strain–displacement relations in Eq. (1), the constitutive relation in Eq. (7), the remaining three compatibility equations, as well as the displacement continuity between each layer yield the displacement expressions in the k^{th} layer of the laminated tube as illustrated in Eqs. (11)–(13):

$$u^{(k)}(x) = \varepsilon_x^0 x \tag{11}$$

$$v^{(k)}(x,r) = \gamma_{x\theta}^0 xr \tag{12}$$

$$w^{(k)}(r) = A_1^{(k)} r^{\lambda(k)} + A_2^{(k)} r^{-\lambda(k)} + \Gamma^{(k)}\varepsilon_x^0 r + \Omega^{(k)}\gamma_{x\theta}^0 r^2 \tag{13}$$

In the above, ε_x^0 and $\gamma_{x\theta}^0$ are axial strain and angle of twist per unit length constants, respectively. $A_1^{(k)}$ and $A_2^{(k)}$ are the integration constants in the k^{th} layer. $\lambda^{(k)}$, $\Gamma^{(k)}$, and $\Omega^{(k)}$ are described in Eq. (14) in terms of components of the transformed stiffness matrix in the k^{th} layer:

$$\lambda^{(\mathrm{k})} = \sqrt{\frac{\overline{C}_{22}^{(\mathrm{k})}}{\overline{C}_{33}^{(\mathrm{k})}}}, \quad \Gamma^{(\mathrm{k})} = \left(\frac{\overline{C}_{12}^{(\mathrm{k})} - \overline{C}_{13}^{(\mathrm{k})}}{\overline{C}_{33}^{(\mathrm{k})} - \overline{C}_{22}^{(\mathrm{k})}}\right), \quad \Omega^{(\mathrm{k})} = \left(\frac{\overline{C}_{26}^{(\mathrm{k})} - 2\overline{C}_{36}^{(\mathrm{k})}}{4\overline{C}_{33}^{(\mathrm{k})} - \overline{C}_{22}^{(\mathrm{k})}}\right) \tag{14}$$

Note that when a layer is made of 0^{o} fiber orientation, the stiffness coefficients $\overline{C}_{16}^{(k)}$, $\overline{C}_{26}^{(k)}$, and $\overline{C}_{36}^{(k)}$ are zero and $\overline{C}_{12}^{(k)} = \overline{C}_{13}^{(k)}$ as well as $\overline{C}_{22}^{(k)} = \overline{C}_{33}^{(k)}$. As such, Eq. (13) is degenerated to become $w^{(k)}(r) = A_1^{(k)} r^{(k)} + A_2^{(k)} r^{-1(k)}$ [13].

For an N-layer laminated tube, there are 2 N + 2 unknown integration constants to be evaluated. Therefore, 2 N + 2 equations are required to solve for the constants. The first four equations written in Eqs. (15)–(18) are obtained from two equations of the force equilibrium with the external loads and two equations from the surface traction boundary conditions. Note that F in Eq. (15) is an axial force, T in Eq. (16) an applied torque, p_i in Eq. (17) a normal traction or internal pressure on the inner surface, and p_o in Eq. (18) a normal traction or external pressure on the outer surface. The remaining 2 N-2 equations can be obtained from N-1 continuity conditions of the interfacial radial stresses, σ_r, and N-1 continuity conditions of the interfacial radial displacements, w, as shown in Eqs. (19) and (20), respectively:

$$\int_{R_0}^{R_N} 2\pi\sigma_x r dr = 2\pi \sum_{k=1}^{N} \int_{R_{k-1}}^{R_k} \sigma_x^{(k)} r dr = F \tag{15}$$

$$\int_{R_0}^{R_N} 2\pi\tau_{x\theta} r^2 dr = 2\pi \sum_{k=1}^{N} \int_{R_{k-1}}^{R_k} \tau_{x\theta}^{(k)} r^2 dr = T \tag{16}$$

$$\sigma_r^{(1)}(R_0) = p_i \tag{17}$$

$$\sigma_r^{(N)}(R_N) = p_0 \tag{18}$$

$$\sigma_r^{(k)}(R_k) = \sigma_r^{(k+1)}(R_k) \qquad (k = 1, 2, 3, \ldots, N-1) \tag{19}$$

$$w^{(k)}(R_k) = w^{(k+1)}(R_{\mathrm{k}}) \qquad (k = 1, 2, 3, \ldots, N-1) \tag{20}$$

Eqs. (15)–(20) give the system of algebraic equations written in matrix form as

$$\begin{bmatrix} k_{11} & k_{12} & k_{13} & \cdots & k_{1,2N+2} \\ k_{21} & k_{22} & k_{23} & \cdots & k_{2,2N+2} \\ k_{31} & k_{32} & k_{33} & \cdots & k_{3,2N+2} \\ k_{41} & k_{42} & k_{43} & \cdots & k_{4,2N+2} \\ \vdots & & & \ddots & \vdots \\ k_{2N+2,1} & k_{2N+2,2} & k_{2N+2,3} & \cdots & k_{2N+2,2N+2} \end{bmatrix} \begin{Bmatrix} F \\ T \\ p_i \\ p_o \\ 0 \\ 0 \\ \vdots \\ 0 \end{Bmatrix} = \begin{Bmatrix} \epsilon_x^0 \\ \gamma_{x\theta}^0 \\ A_1^{(1)} \\ A_2^{(1)} \\ \vdots \\ A_1^{(N)} \\ A_2^{(N)} \end{Bmatrix} \tag{21}$$

where k_{ij} $(i, j = 1, 2, 3, \ldots, 2N + 2)$ are the coefficients obtained from the equations above. By solving Eq. (21), the constants $\epsilon_x^0, \gamma_{x\theta}^0,$ and $A_1^{(1)}, A_2^{(1)}, \ldots, A_1^{(N)}, A_2^{(N)}$ can be obtained. Subsequently, all displacements, strains, and stresses are calculated by using Eqs. (11)–(13), (1), and (7), respectively.

3. Formulation of an equivalent lap joint model

3.1. Derivation of governing equations

All geometric parameters of a perfectly bonded tubular lap joint are shown in **Figure 1(b)**. The adhesive is assumed to be isotropic and linearly elastic. The adhesive thickness t_a is considered to be very thin compared to the adherend thicknesses, and thus, the outer radius of part 1 R_{1o} is approximately the same as the inner radius of part 2, R_{2i}. In addition, there are only three out-of-plane stress components mainly contributed in the adhesive: hoop shear stress $\tau_{\theta r}^a,$ longitudinal shear stress τ_{xr}^a, and radial normal stress σ_r^a. These stresses in the adhesive are treated to be uniform through the adhesive thickness. Applied torque T; applied axial force F; internal pressure exerted on the inner surface of adherend part 1, p_i or written specifically as p_{1i}; and external pressure exerted on the outer surface of adherend part 2, p_o or $p_{2o},$ are all included in the following formulation.

In order to derive the governing equations, let us initially consider the torque transmission through a coupler joint. The applied torque T is assumed to distribute only in the adherend part 1 and adherend part 2 as denoted as T_1 and T_2, respectively. Hence, the applied torque T can be written as

$$T = T_1 + T_2 \tag{22}$$

To determine the variation of the T_2 along the bonding length, the adherend 2 is divided into elements with an infinitesimal length dx. The equilibrium between the resultant torque in the element and the adhesive hoop shear stress can be expressed as follows:

$$\frac{1}{2\pi R_{2i}^2}\frac{dT_2(x)}{dx} = \tau_{\theta r}^a = G^a \gamma_{\theta r}^a \tag{23}$$

In Eq. (23), G^a is shear modulus of adhesive. By considering the deformation of an adhesive element on a cross-sectional plane in the overlap region of the perfectly bonded joint, the kinematic condition in the adhesive can be written as

$$\gamma_{\theta r}^a = \frac{v_{2i} - v_{1o}}{t_a} \tag{24}$$

and its derivative with respect to x is.

$$\frac{d\gamma_{\theta r}^a}{dx} = \frac{\gamma_{x\theta}^{2i} - \gamma_{x\theta}^{1o}}{t_a} \tag{25}$$

Combining Eqs. (23) and (25) yields the first governing equation:

$$\frac{d^2T_2(x)}{dx^2} = \frac{2\pi R_{2i}^2 G^a}{t_a}\left(\gamma_{x\theta}^{2i} - \gamma_{x\theta}^{1o}\right) \tag{26}$$

Next, consider equilibrium of resultant axial force. When the joint is subjected to tension or compression loads, the resultant axial force in the adherend 1, F_1, and in adherend 2, F_2, are produced at any given cross section in the overlap region, similar to Eq. (22). The force equilibrium is

$$F = F_1 + F_2 \tag{27}$$

The variation of the F_2 along the length can be examined by considering an infinitesimal elements in adherend part 2 with the differential length dx. The equilibrium between resultant axial force in the element and the adhesive longitudinal shear stress τ_{xr}^a can consequently be expressed as follows:

$$\frac{1}{2\pi R_{2i}}\frac{dF_2(x)}{dx} = \tau_{xr}^a = G^a\gamma_{xr}^a \tag{28}$$

By considering compatibility of the joint, it can be shown that.

$$\gamma_{xr}^{a} = \frac{u_{2i} - u_{1o}}{t_a} \text{ or } \frac{d\gamma_{xr}^{a}}{dx} = \frac{\varepsilon_x^{2i} - \varepsilon_x^{1o}}{t_a} \tag{29}$$

Combining Eqs. (28) and (29) yields the axial force governing equation:

$$\frac{d^2F_2(x)}{dx^2} = \frac{2\pi R_{2i} G^a}{t_a}\left(\varepsilon_x^{2i} - \varepsilon_x^{1o}\right) \tag{30}$$

Next, interacting through the adhesive thickness, the resultant normal traction acting on the outer surface of adherend 1, p_{1o}, and that exerting on the inner surface of adherend 2, p_{2i}, are generated. Under the assumption of thin adhesive layer, the resultant normal tractions p_{1o} and p_{2i} are related to each other as

$$p_{1o} = p_{2i} \tag{31}$$

Lastly, instead of directly equating adhesive radial normal stress to normal traction in (31), σ_r^a can be more accurately determined by the equilibrium equation in cylindrical coordinates of the adhesive layer showing in Eq. (32):

$$\frac{\partial\sigma_r}{\partial r} + \frac{1}{r}(\sigma_r - \sigma_\theta) + \frac{1}{r}\frac{\partial\tau_{\theta r}}{\partial\theta} + \frac{\partial\tau_{xr}}{\partial x} = 0 \tag{32}$$

With the conditions of axisymmetry, the equilibrium equation is reduced to

$$\frac{1}{R_{2i}}\left(\sigma_r^a - \sigma_\theta^a\right) + \frac{\partial \tau_{xr}^a}{\partial x} = 0 \tag{33}$$

According to the study conducted in [6], σ_θ^a is observed to have the same distribution as σ_r^a so they are legitimately regarded as being proportional to each other via adhesive normal stress ratio α. Their relation can be mathematically expressed in Eq. (34):

$$\sigma_\theta^a = \alpha \sigma_r^a \tag{34}$$

As a consequence, the equilibrium equation in Eq. (32) can then be written as

$$\sigma_r^a = -\frac{1}{2\pi(1-\alpha)} \frac{d^2 F_2(x)}{dx^2} \tag{35}$$

3.2. Implementation of elasticity theory for adherends

The two governing equations Eqs. (26) and (30) have already been formulated to determine resultant loads in adherend part 2 of an adhesive-bonded-coupler joint. The resultant loads in adherend part 1 can be then calculated easily by using Eqs. (22) and (27) after all internal loads in adherend part 2 are evaluated. However, related through Eq. (21), the two equations are coupled and need to be solved altogether. To aptly deal with this complicated condition, the problem is separated into primary and secondary effects. When the joint is subjected to torsion, the hoop shear stress in the adhesive $\tau_{\theta r}^a$ is primary and dominant compared to the other adhesive stresses as discussed in [8, 10, 13], whereas in the case of the joint being under an application of longitudinal force, or external and internal pressure, the adhesive longitudinal shear stress τ_{xr}^a and adhesive radial normal stress σ_r^a are comparatively crucial [20]. By neglecting the secondary stress components and the corresponding resultant internal loads in the early calculation stage, the problem is then uncoupled and can be readily solved for the primary variables. The initially excluded stress components are later recovered by using the obtained solutions in the coupled set of governing equations.

First, further modification of the torque governing equation of Eq. (26) is performed, adherend in-plane shear strains $\gamma_{x\theta}^{1o}$ and $\gamma_{x\theta}^{2i}$ must be expanded in terms of the internal resultant loads. It can be seen that they are equal to $\gamma_{x\theta}^{01} R_{1o}$ and $\gamma_{x\theta}^{02} R_{2i}$, respectively, where $\gamma_{x\theta}^{01}$ and $\gamma_{x\theta}^{02}$ are denoted for $\gamma_{x\theta}^{0}$ of adherend parts 1 and 2. Utilizing Eq. (21) yields the relations:

$$R_{1o}\left(k_{21}^1 F_1 + k_{22}^1 T_1 + k_{23}^1 p_{1i} + k_{24}^1 p_{1o}\right) = \gamma_{x\theta,F}^{1o} F_1 + \gamma_{x\theta,T}^{1o} T_1 + \gamma_{x\theta,pi}^{1o} p_{1i} + \gamma_{x\theta,po}^{1o} p_{1o} = \gamma_{x\theta}^{1o} \tag{36}$$

$$R_{2i}\left(k_{21}^2 F_2 + k_{22}^2 T_2 + k_{23}^2 p_{2i} + k_{24}^2 p_{2o}\right) = \gamma_{x\theta,F}^{2i} F_2 + \gamma_{x\theta,T}^{2i} T_2 + \gamma_{x\theta,pi}^{2i} p_{2i} + \gamma_{x\theta,po}^{2i} p_{2o} = \gamma_{x\theta}^{2i} \tag{37}$$

where quantities k_{2X}^1 and k_{2X}^2, where $X = 1, 2, 3$, and 4 are the first four elements compliances in the second row of matrix $[k]$ in Eq. (21). Superscripts 1 and 2 are defined for adherend parts 1 and 2, respectively. $\gamma_{x\theta,F}^{1o}$, $\gamma_{x\theta,T}^{1o}$, $\gamma_{x\theta,pi}^{1o}$, $\gamma_{x\theta,po}^{1o}$, $\gamma_{x\theta,F}^{2i}$, $\gamma_{x\theta,T}^{2i}$, $\gamma_{x\theta,pi}^{2i}$, and $\gamma_{x\theta,po}^{2i}$ are in-plane shear strains per unit load on the outer interfacial surface of adherend part 1 and inner interfacial surface of adherend part 2, respectively.

By substituting Eqs. (36) and (37) into the governing equation Eq. (26) and utilizing Eqs. (22), (27), and (31), the governing equation in term of T_2 becomes

$$\frac{d^2T_2(x)}{dx^2} = K_F F_2(x) + K_T T_2(x) + K_p p_{2i}(x) + K_C \tag{38}$$

where the parameters K_F, K_T, K_p, and K_C are.

$$\begin{aligned} K_F &= \frac{2\pi R_{2i}^2 G^a}{t_a}\left(\gamma_{x\theta,F}^{2i} + \gamma_{x\theta,F}^{1o}\right), K_T = \frac{2\pi R_{2i}^2 G^a}{t_a}\left(\gamma_{x\theta,T}^{2i} + \gamma_{x\theta,T}^{1o}\right), \\ K_p &= \frac{2\pi R_{2i}^2 G^a}{t_a}\left(\gamma_{x\theta,pi}^{2i} - \gamma_{x\theta,po}^{1o}\right), \qquad K_C = \frac{2\pi R_{2i}^2 G^a}{t_a}\left(\gamma_{x\theta,po}^{2i} p_o - \gamma_{x\theta,pi}^{1o} p_i - \gamma_{x\theta,F}^{1o} F - \gamma_{x\theta,T}^{1o} T\right) \end{aligned} \tag{39}$$

Accompanying with the boundary conditions of Eq. (40), which are implied that torque in adherend part 2 is zero at $x = 0$ and fully transmitted at $x = L$, Eq. (38) is well-defined for solving resultant torque in the adherend part 2,T_2:

$$T_2(0) = 0, \qquad T_2(L) = T \tag{40}$$

Second, analogous to Eqs. (36) and (37), adherend in-plane normal strains ε_x^{1o} and ε_x^{2i} must also be written in terms of the internal resultant loads. Again, using the expression in Eq. (21), the following expressions are obtained:

$$\left(k_{11}^1\right)F_1 + \left(k_{12}^1\right)T_1 + \left(k_{13}^1\right)p_{1i} + \left(k_{14}^1\right)p_{1o} = \varepsilon_{x,F}^{1o}F_1 + \varepsilon_{x,T}^{1o}T_1 + \varepsilon_{x,pi}^{1o}p_{1i} + \varepsilon_{x,po}^{1o}p_{1o} = \varepsilon_x^{1o} \tag{41}$$

$$\left(k_{11}^2\right)F_2 + \left(k_{12}^2\right)T_2 + \left(k_{13}^2\right)p_{2i} + \left(k_{14}^2\right)p_{2o} = \varepsilon_{x,F}^{2i}F_2 + \varepsilon_{x,T}^{2i}T_2 + \varepsilon_{x,pi}^{2i}p_{2i} + \varepsilon_{x,po}^{2i}p_{1o} = \varepsilon_x^{2i} \tag{42}$$

In the above, k_{1X}^1 and k_{1X}^2, where $X = 1, 2, 3,$ and 4 are the first four elements in the first row of matrix $[k]$ in Eq. (21). Superscripts 1 and 2 are defined for adherend parts 1 and 2, respectively. $\varepsilon_{x,F}^{1o}$, $\varepsilon_{x,T}^{1o}$, $\varepsilon_{x,pi}^{1o}$, $\varepsilon_{x,po}^{1o}$ $\varepsilon_{x,F}^{2i}$, $\varepsilon_{x,T}^{2i}$, $\varepsilon_{x,pi}^{2i}$, and $\varepsilon_{x,po}^{2i}$ are newly denoted to indicate the physical meaning of the parameters. They represent the in-plane normal strains due to unit load on the adhesive-interfacial surface in the adherends. The unit load quantities are distinguished by after-comma subscripts F, T, or p. Quantities ε_x^{1o} and ε_x^{2i} are ε_x^0 of adherends 1 and 2, respectively.

Combining the governing equations Eqs. (30), (41), and (42), as well as the load equilibriums in Eqs. (22), (27), and (31), yields a new form of the axial force governing equation:

$$\frac{d^2F_2(x)}{dx^2} = k_F F_2(x) + k_T T_2(x) + k_p p_{2i}(x) + k_C \tag{43}$$

where the parameters k_F, k_T, k_p, and k_C are.

$$\begin{aligned} k_F &= \frac{2\pi R_{2i} G^a}{t_a}\left(\varepsilon_{x,F}^{2i} + \varepsilon_{x,F}^{1o}\right), k_T = \frac{2\pi R_{2i} G^a}{t_a}\left(\varepsilon_{x,T}^{2i} + \varepsilon_{x,T}^{1o}\right) \\ k_p &= \frac{2\pi R_{2i} G^a}{t_a}\left(\varepsilon_{x,\mathrm{pi}}^{2i} - \varepsilon_{x,po}^{1o}\right), \quad k_C = \frac{2\pi R_{2i} G^a}{t_a}\left(\varepsilon_{x,po}^{2i} p_o - \varepsilon_{x,pi}^{1o} p_i - \varepsilon_{x,F}^{1o} F - \varepsilon_{x,T}^{1o} T\right) \end{aligned} \tag{44}$$

To specify the boundary conditions of Eq. (43), one can consider the disappearance of F_2 at $x = 0$. This is because the left end surfaces of the adherend are normal traction-free. The right end at $x = L$ on the other hand must take the full axial load F if there exists the application of external axial load. Thus, in the mathematical form, these boundary conditions are as follows:

$$F_2(0) = 0, \qquad F_2(L) = F \tag{45}$$

Finally, it should be noted that the occurrence of p_{2i} in Eq. (43) is closely related with the existence of F_2 because the tensile or compressive loading can induce the peeling traction. Therefore, p_{2i} in the equation is considered as unknown. However, it is possible to find the approximated relation between the two variables by letting T_2 and p_{2i} be zero; F_2 then can be evaluated and expressed in Eq. (46):

$$F_2(x) = a_0 e^{\sqrt{k_F}x} + b_0 e^{-\sqrt{k_F}x} - \frac{k_C}{k_F} \tag{46}$$

where a_0 and b_0 are integration constants.

Reinstating the resultant normal traction p_{2i} and substituting Eq. (46) into Eq. (43), it is found that p_{2i} can be simply estimated as

$$p_{2i} \approx a_1 e^{\sqrt{k_F}x} + b_1 e^{-\sqrt{k_F}x} \tag{47}$$

in which, a_1 and b_1 are unknown parameters. In order to determine these two parameters, two more boundary conditions are required from zero longitudinal shear stress τ^a_{xr} in the adhesive layer at left and right ends as shown in Eq. (48):

$$\left.\frac{dF_2}{dx}\right|_{x=0} = 0, \qquad \left.\frac{dF_2}{dx}\right|_{x=L} = 0 \tag{48}$$

Up to this point, the unified formulation of an analysis of adhesive-bonded coupler joint has been developed. The model can be universally used to determine the stresses in the adhesive layer for any particular load case previously mentioned. To elaborate the applicability of the model for each loading condition, i.e., torsion, axial, or external and internal pressure, the pertinent details are given below:

- For torsional load, the secondary variables, namely, F_2 and p_{2i}, are initially neglected in Eq. (38). In addition, $F = p_{1i} = p_{2o} = 0$. Consequently, T_2 and $\tau^a_{\theta r}$ can be evaluated. Subsequently, F_2, τ^a_{xr}, and σ^a_r and can be recovered and computed by employing the full form of Eqs. (43) and (47), (28), and (35), respectively.
- For axial load, the secondary variable T_2 is initially neglected. Additionally, $T = p_{1i} = p_{2o} = 0$. The primary variables F_2, τ^a_{xr}, and σ^a_r are solved by using the governing equation, Eqs. (43), (47), (28), and (35). T_2 and $\tau^a_{\theta r}$ is later calculated from the full form of Eqs. (38) and (23), respectively.

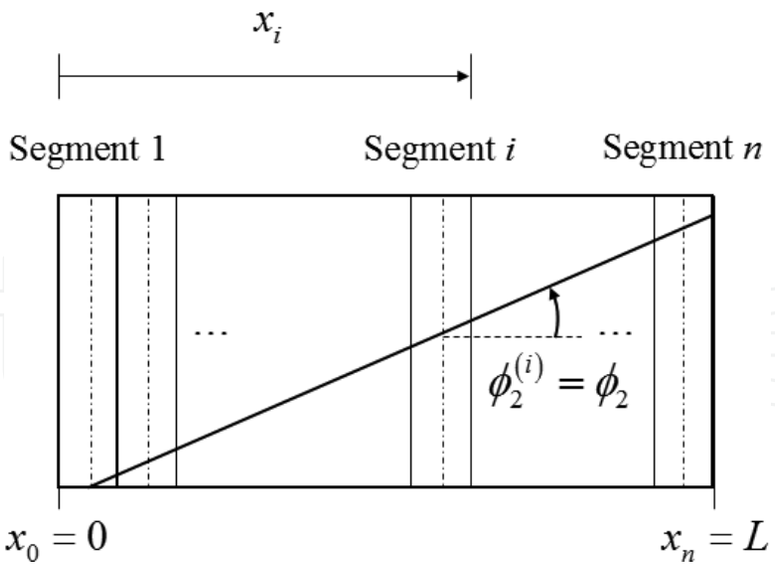

Figure 3. A segment at a certain axial position x.

- For external and internal pressure, the secondary variable T_2 is firstly omitted. In this case $T = F = 0$. If only external pressure is present, $p_{1i} = 0$, whereas if only internal pressure exists, $p_{2o} = 0$. The first variables F_2, τ_{xr}^a, and σ_r^a are solved by using the governing equation, Eqs. (43), (47), (28), and (35). T_2 and $\tau_{\theta r}^a$ can be later recovered the same way as those for the axial load.

3.3. Finite segment solution for evaluating adherend stresses

As previously discussed, all resultant loads in adherend parts 1 and 2 can be obtained as functions of x-coordinate. Equipped with the elasticity solution discussed in Section 2, the stress analysis in the adherends can be performed by utilizing a technique so-called finite-segment method (FSM) developed in [13]. The joint in the overlap region is divided into n numbers of segment as illustrated in **Figure 3** to take care of the axial variation of the resultant loads. The corresponding resultant loads of each segment are then approximated to be constant, and thus, application of the theory delineated in the previous section is valid. For a composite coupler, the fiber angle in the adherend part 2 is denoted as $\varnothing_2$. Note that if the stresses in adherend part 2 are evaluated, the internal pressure p_i in Eq. (21) or equivalently p_{2i} should be substituted by the radial normal stress σ_r^a obtained from Eq. (35) for more accurate results. Likewise, the procedure must be done for p_{1o} if adherend part 1 is considered. When all of the resultant loads in Eq. (21) in each segment are completely determined, stresses in both adherends can be finally computed and analyzed.

4. Results

Presented in this section are some sample computational results of the model developed. The numerical calculation is performed by using software MATHEMATICA™. The validation of

the model is not given herein, since it has already been shown in [13] and [20]. Adhesive-bonded tubular joints with isotropic inner adherend and symmetric-balanced four-layer stacking sequence $[\pm\varnothing_2]_s$ couplers are selected for consideration. The reference joint geometry is given with parameters $R_{10} = 10$, $t_1 = 5$, $t_2 = 5$, $t_a = 0.1$, and $L = 40$ mm. The adherend part 1 is made of steel, whereas the adherend part 2 is fabricated from carbon fiber-reinforced plastic. Epoxy is used as the adhesive material. The material properties of the joints are listed in **Table 1**. Adhesive normal stress ratio, α, is set to be 20 because it has shown to provide accurate predictions of adhesive radial stresses [20]. In the following computational results, the adhesive stresses in the coupler joint are normalized by the average applied stress in each loading case, because the dimensionless stresses are readily exploited to identify the level of load distribution intensity in the joint.

4.1. Torsional loading

In the case of torsional loading, the joints are assumed to have a torque of 1 N.m as an input without loss of generality. Also, the adhesive mean shear stress τ_m^a in Eq. (49) is utilized to normalize the induced adhesive hoop shear stress in the coupler joint:

$$\tau_m^a = \frac{T}{2\pi R_{2i}^2 L} \tag{49}$$

The resultant torque of the adherend part 2 and normalized adhesive hoop shear stress can be calculated and plotted in **Figures 4** and **5**, respectively. It can be noticed that the joints considered develop the nonconstant slopes in **Figure 4** with relatively high torque gradients at both ends. This is equivalent to the peak adhesive hoop shear stresses at x = 0 and L in **Figure 5**. Note that the torque and stress distributions for $\varnothing_2 = 0^\circ$ and 30° are identical to those for 90° and 60°, respectively, so they cannot be clearly seen. In addition, since the fiber orientation of 45° is the most suitable angle to withstand the in-plane shear loads, the coupler with $\varnothing_2 = 45^\circ$ provides the lowest magnitude of $\tau_{\theta r}^a$ as expected.

Stress distributions in the composite coupler are illustrated in **Figure 6** for the case of $\varnothing_2 = 30^o$. The normal stress in the fiber direction σ_{11} in **Figure 6(a)** is the dominant stress component compared to those in the other directions. The radial normal stress σ_{33} illustrated in **Figure 6(b)** is relatively small at x = 0 mm and noticeably larger at x = 40 mm. In addition, σ_{33} at adhesive-

Properties	Epoxy (adhesive)	Steel (adherend 1)	Carbon/epoxy (adherend 2)
E_1 (GPa)	1.30	200.00	128.00
E_2, E_3 (GPa)	1.30	200.00	10.00
G_{12}, G_{13} (GPa)	0.46	76.90	50.00
G_{23} (GPa)	0.46	76.90	50.00
υ_{12}, υ_{13}	0.41	0.30	0.28
υ_{23}	0.41	0.30	0.47

Table 1. Mechanical properties of materials in the principle material coordinate [20].

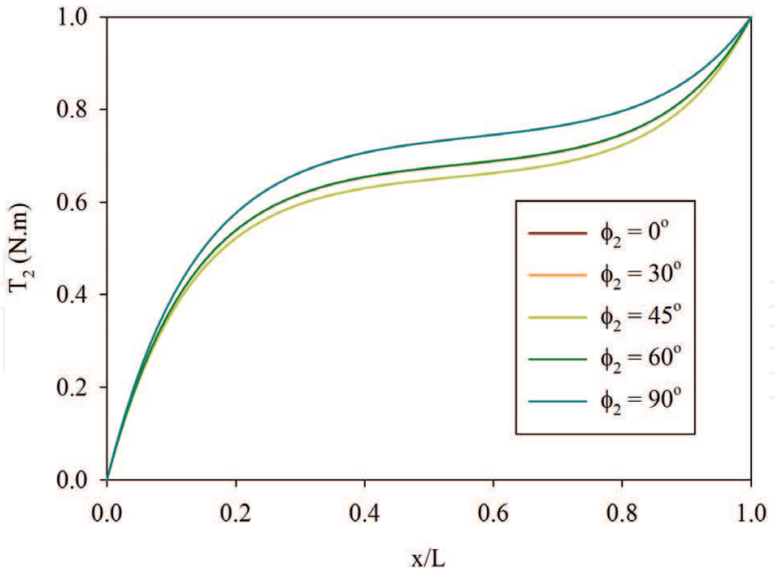

Figure 4. Torque distribution in adherend part 2 of composite coupler joint subjected to torsion.

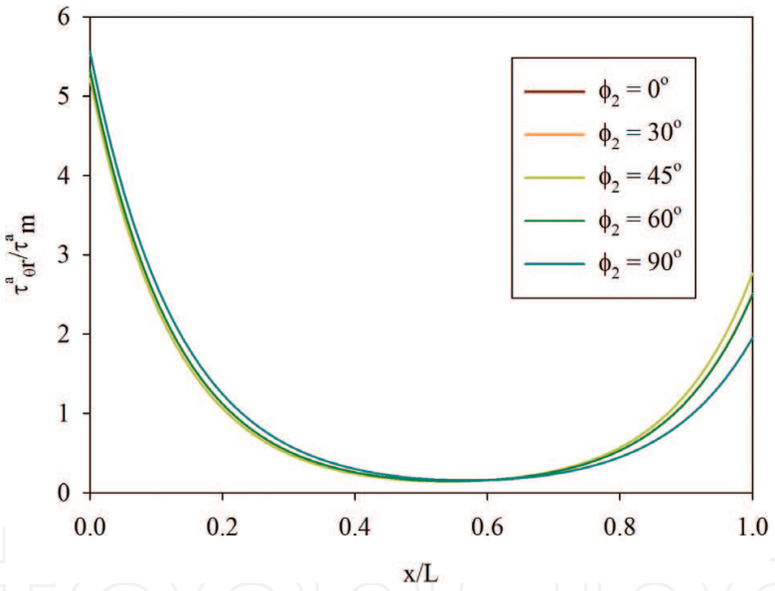

Figure 5. Adhesive hoop shear stress distribution of composite coupler joint subjected to torsion.

coupler interface r = 10.1 mm or σ_r^a is also minimal because of being the secondary effect. Note that the number of segments used to calculate the stresses in **Figure 6** is 40. Finally, the figure shows that the developed model is capable of capturing the variation of these two stress components through the coupler thickness thanks to the advantage of the elasticity theory.

4.2. Axial loading

When the coupler joints are subjected to an axial loading, a tension force with the magnitude of 1 N is used in calculation. For this particular case, the adhesive mean shear stress τ_m^a in Eq. (50)

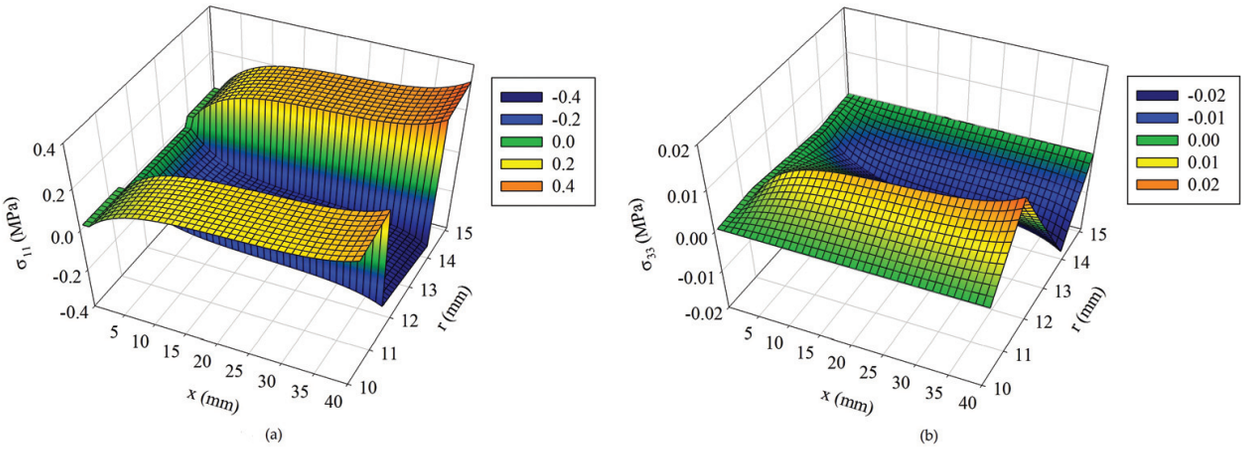

Figure 6. Distribution of stresses in composite coupler subjected to torsion.

is adopted to normalize the induced longitudinal shear stress and radial normal stress in the adhesive. Same as above, the normalized stresses can be utilized to indicate the distribution intensity of load transfer within the joints:

$$\tau_m^a = \frac{F}{2\pi R_{2i} L} \tag{50}$$

Figures 7 and **8** show the effect of fiber orientation on the distributions of F_2 and τ_{xr}^a along the overlap region, respectively. Observation in **Figure 8** reveals that by adjusting fiber orientation, the composite coupler can generate mostly uniform load transmission in the central bonding region. The internal forces F_2 of **Figure 7** in that region concomitantly reveal linear relationships with the spatial coordinate x/L. The optimum fiber angle $\varnothing_2$ is about 30°, which provides the lowest maximum τ_{xr}^a/τ_m^a of 1.2. **Figure 9** shows the radial normal stress in the adhesive. Generally speaking, the smaller peak of τ_{xr}^a/τ_m^a, the lower magnitude of σ_r^a/τ_m^a.

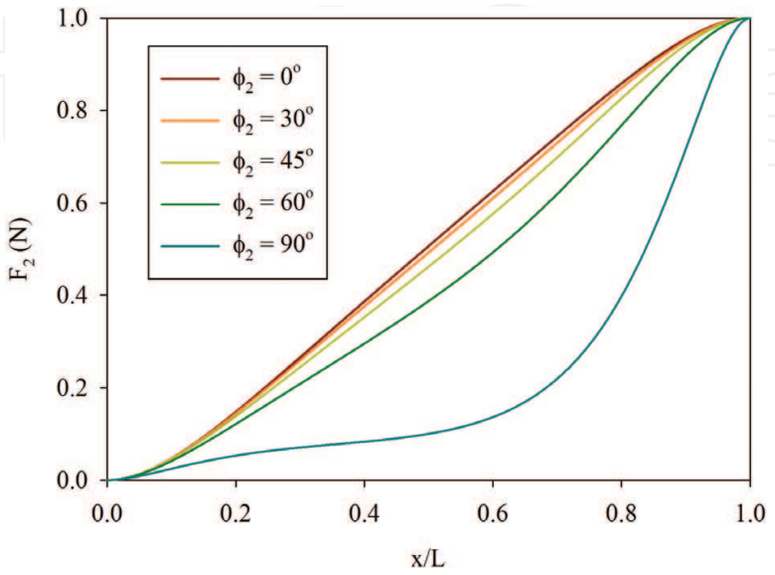

Figure 7. Force distribution in adherend part 2 of composite coupler joint subjected to tension.

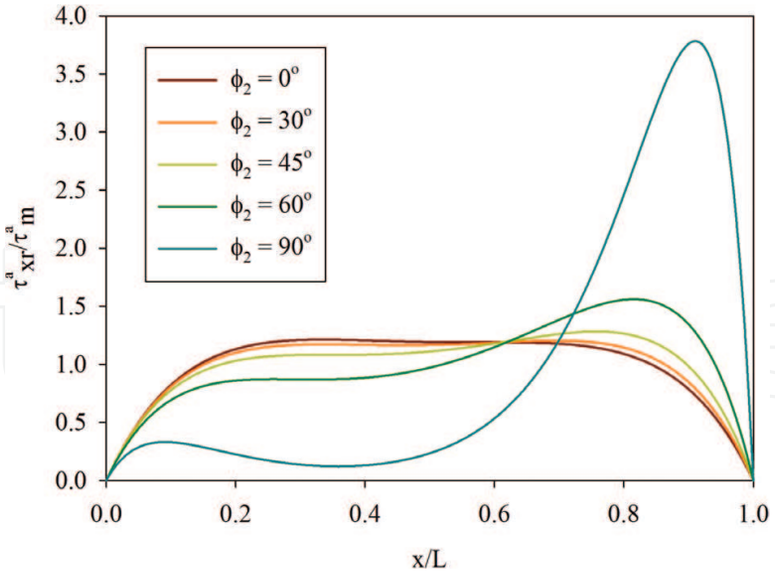

Figure 8. Adhesive axial shear stress distribution of composite coupler joint subjected to tension.

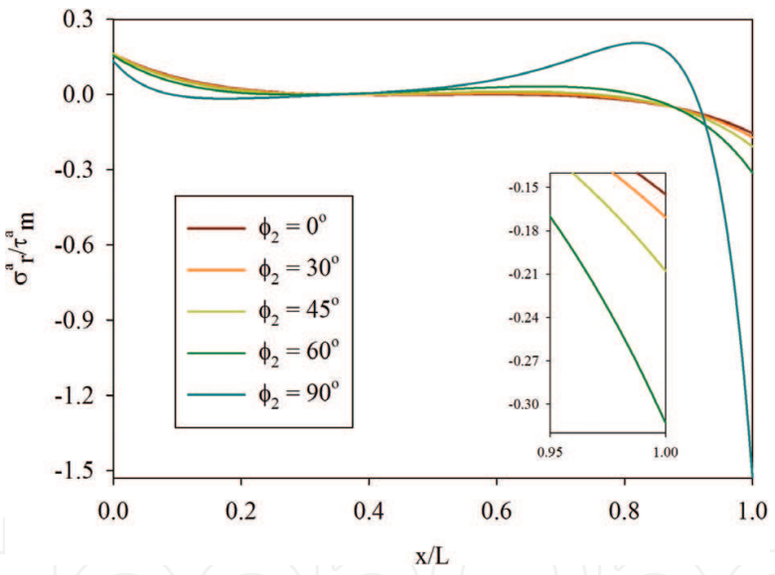

Figure 9. Interfacial radial stress distribution of composite coupler joint subjected to tension.

Figure 10 shows the normal stresses σ_{11} and σ_{33} of adherend part 2 in the principal material coordinate system, when the fiber orientation is equal to 30°. It can be seen from the figure that under the application of the axial force, σ_{11} is vanished at the left of the bonding region due to the traction-free surface, while σ_{33} is disappeared on the outermost area of the coupler. The stress in the fiber direction σ_{11} steadily attains the same maximum value along the bond length in all laminae of composite coupler. The radial normal stress σ_{33}, which is induced from the resultant axial force, is highest at the adhesive-coupler interface.

4.3. Pressure loading

Lastly, for the case of pressure loads, 1 MPa internal pressure is exerted inside the adherend part 1, but no external pressure is present on the outer surface of the adherend part 2. The

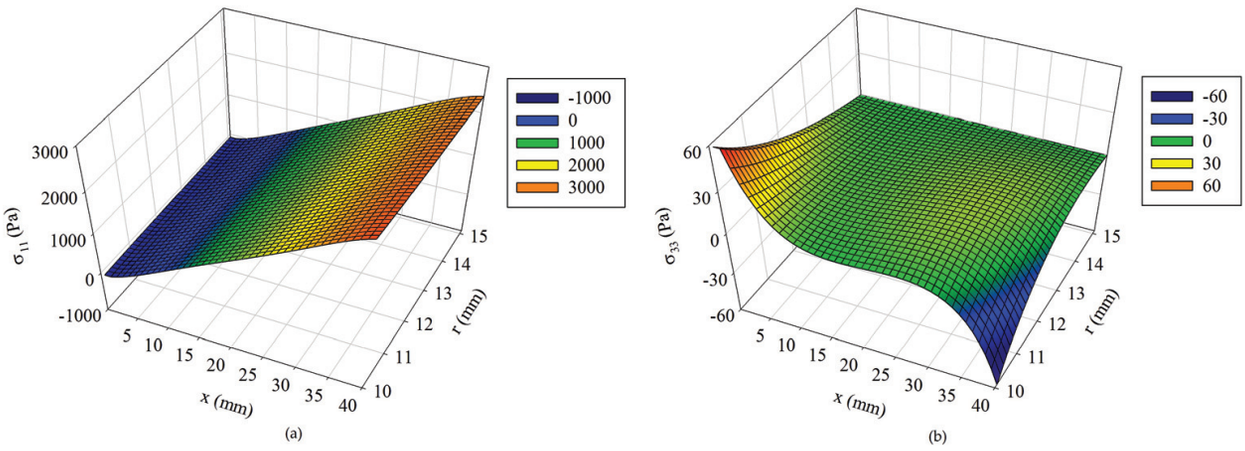

Figure 10. Distribution of stresses in composite coupler subjected to tension.

adhesive longitudinal shear stress and adhesive radial normal stress can then be normalized by the internal pressure to form the dimensionless variables.

Figures 11 and **12** show the effect of fiber orientation on the distributions of F_2 and τ_{xr}^a along the overlap region, respectively. **Figure 11** indicates that peak values of F_2 are generated in the central region of the composite couplers, but their values are null at both ends. The longitudinal shear stresses in adhesive τ_{xr}^a in **Figure 12** illustrate the antisymmetric characteristic along the bond length. It can be seen that the optimum fiber angle $\emptyset_2$ is 90°. This fiber orientation delivers the lowest maximum τ_{xr}^a/p_i of 0.6. **Figure 13** shows the radial normal stress in the adhesive. Interestingly, the values of σ_r^a are reduced by four to five times compared to the internal pressure applied over the whole range of the fiber angles considered.

The normal stresses σ_{11} and σ_{33} of adherend part 2 in the principal material coordinate system, when the fiber orientation are equal to 30°, are displayed in **Figure 14**. It can be noticed that under the application of the uniform internal pressure with 1 MPa magnitude, σ_{11} is

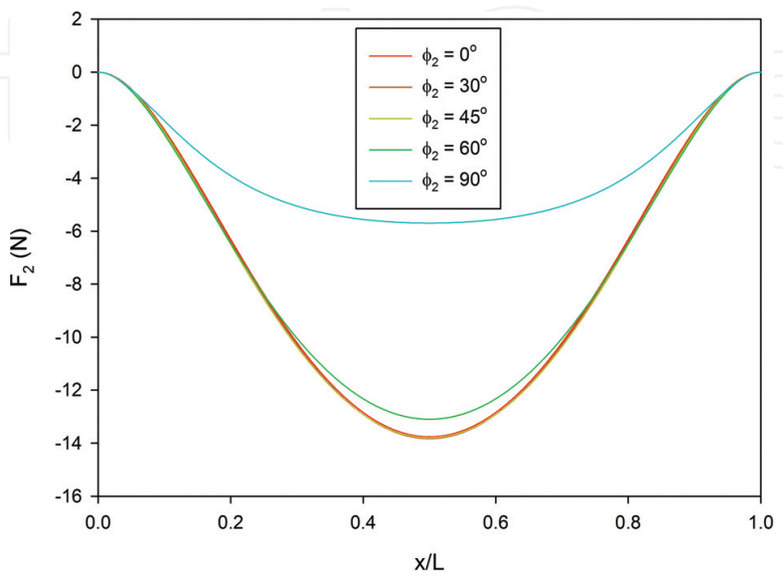

Figure 11. Force distribution in adherend part 2 of composite coupler joint subjected to internal pressure.

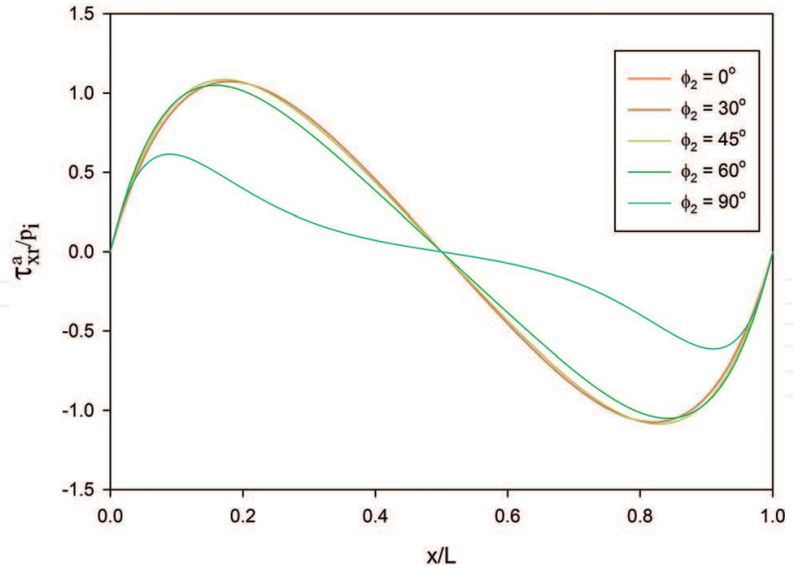

Figure 12. Adhesive axial shear stress distribution of composite coupler joint subjected to internal pressure.

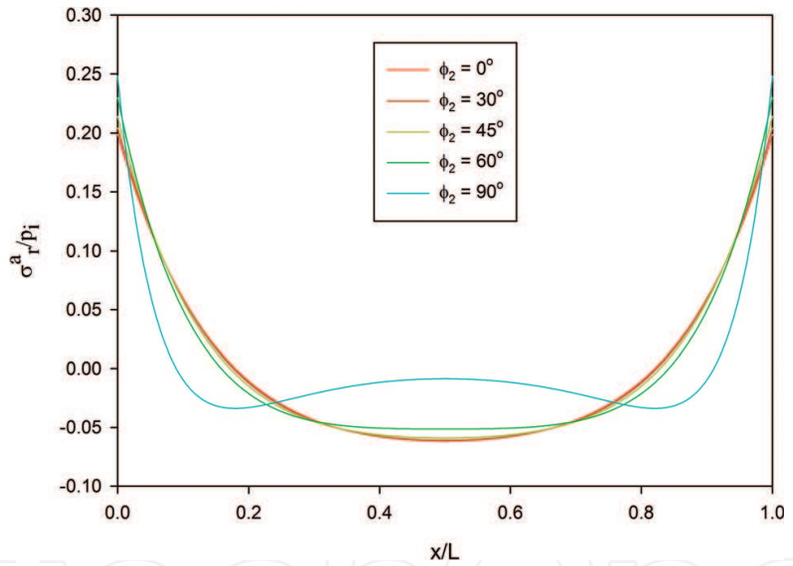

Figure 13. Interfacial radial stress distribution of composite coupler joint subjected to internal pressure.

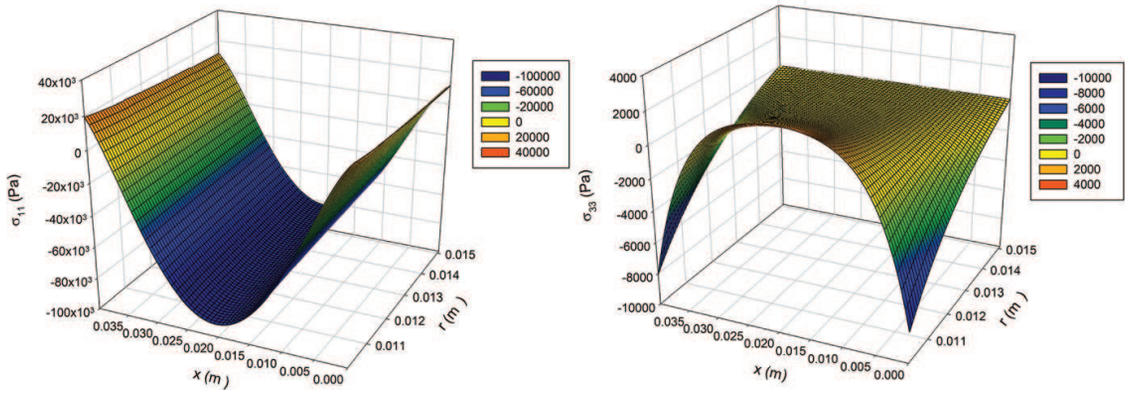

Figure 14. Distribution of stresses in composite coupler subjected to internal pressure.

maximum at the mid-length of bonding region, whereas σ_{33} is peak at $x = 0$ and 40 mm on the adhesive-adherend interface.

5. Conclusions

A unified mathematical model for predicting the joint stresses of the adhesive-bonded tubular-coupler joints or the equivalent bonded-lap joints under several types of load is formulated. The inner and outer adherends can be considered as an isotropic material, orthotropic material, or a laminated composite, whose fiber angle is constant along the tube axis. They are modeled as three-dimensional body and satisfied the equilibrium, kinematic, and constitutive equations in theory of elasticity. The adhesive is only treated to be a very thin isotropic elastic material with relative low modulus, and thus, merely three out-of-plane stress components are present. The finite-segment method is developed to compute adherend stresses in each small portion of the coupler. The analytical results obtained indicate the viability of the model for many joint conditions and configurations. The model can be used conveniently in the preliminary process of the joint design, which is usually critical in huge, complex, or integrated structures.

Author details

Sontipee Aimmanee

Address all correspondence to: sontipee.aim@kmutt.ac.th

Advanced Materials and Structures Laboratory (AMASS), Department of Mechanical Engineering, Faculty of Engineering, King Mongkut's University of Technology Thonburi (KMUTT), Bangmod, Bangkok, Thailand

References

[1] Lubkin JL, Reissner E. Stress distribution and design for adhesive lap joints between circular tubes. Transactions of ASME. 1956;**78**:1213-1221

[2] Adams R, Peppiatt N. Stress analysis of adhesive-bonded tubular lap joints. Journal of Adhesion. 1977;**9**:1-18

[3] Allman DJ. A theory for elastic stresses in adhesive bonded lap joints. The Quarterly Journal of Mechanics and Applied Mathematics. 1977;**30**:415-436

[4] Shi YP, Cheng S. Analysis of adhesive-bonded cylindrical lap joints subjected to axial load. Journal of Engineering Mechanics. 1993;**119**(3):584-602

[5] Nemes O, Lachaud F, Mojtabi A. Contribution to the study of cylindrical adhesive joining. International Journal of Adhesion and Adhesives. 2006;**26**:474-448

[6] Kumar S, Khan MA. An elastic solution for adhesive stresses in multi-material cylindrical joints. International Journal of Adhesion and Adhesives. 2016;**64**:142-152

[7] Kumar S. Analysis of tubular adhesive joints with a functionally modulus graded bondline subjected to axial loads. International Journal of Adhesion and Adhesives. 2009;**29**:785-795

[8] Volkersen O. Recheraches sur la theorie des assemblages colles. Construction Metallique. 1965;**4**:3-13

[9] Pugno N, Surace G. Tubular bonded joint under torsion: Theoretical analysis and optimization for uniform torsional strength. Journal of Strain Analysis. 2001;**36**(1):17-24

[10] Xu W, Li G. Finite difference three-dimensional solution of stresses in adhesively bonded composite tubular joint subjected to torsion. International Journal of Adhesion and Adhesives. 2010;**30**:191-199

[11] Nonlinear OJH. Analysis of adhesive bonded tubular single-lap joints for composites in torsion. Composites Science and Technology. 2007;**67**:1320-1329

[12] Spaggiari A, Dragoni E. Regularization of torsional stresses in tubular lap bonded joints by means of functionally graded adhesives. International Journal of Adhesion and Adhesives. 2014;**53**:23-28

[13] Aimmanee S, Hongpimolmas P. Stress analysis of adhesive-bonded tubular-coupler joints with optimum variable-stiffness composite adherend under torsion. Composite Structures. 2017;**164**:76-89

[14] Terekhova LP, Skoryi IA. Stresses in bonded joints of thin cylindrical shells. Strength of Materials. 1972;**4**(10):1271-1274

[15] Baishya N, Das RR, Panigrahi SK. Failure analysis of adhesively bonded tubular joints of laminated FRP composites subjected to combined internal pressure and torsional loading. Journal of Adhesion Science and Technology. 2017;**31**(19-20)

[16] Zhang Y, Qin TY, Noda, NA, Duan ML. Strength analysis of adhesive joints of riser in deep sea environment loadings. Applied Adhesion Science. 2013;**1**:1-9

[17] Apalak MK. Stress analysis of an adhesively bonded functionally graded tubular single lap joint subjected to an internal pressure. Science and Engineering of Composite Materials. 2006;**13**(3):183-211

[18] Herakovich CT. Mechanics of Fibrous Composites. USA: John Wiley& Sons, Inc; 1998

[19] Carlucci D, Payne N, Mehmedagic I. Small Strain Compatibility Conditions of an Elastic Solid in Cylindrical Coordinates. New Jersey: U.S. Army ARDEC; 2013. pp. 1-12

[20] Aimmanee S, Hongpimolmas P, Ruangjirakit K. Simplified analytical model for adhesive-bonded tubular joints with isotropic and composite adherends subjected to tension. International Journal of Adhesion and Adhesive (submitted)

IntechOpen